Unravelling the Role of an Aqueous Environment on the Electronic Structure and Ionisation of Phenol Using Photoelectron Spectroscopy

Jamie W. Riley, Bingxing Wang, Joanne L. Woodhouse, Mariana Assmann, Graham A. Worth and Helen H. Fielding*

Department of Chemistry, University College London, 20 Gordon Street, London, WC1H 0AJ, UK

E-mail: h.h.fielding@ucl.ac.uk

*To whom correspondence should be addressed

Supplementary Information

1 Experimental methods

1.1 Molecular-beam photoelectron spectrometer

Our molecular beam velocity-map imaging (VMI) photoelectron spectrometer has been described in detail elsewhere.[1] Briefly, a molecular beam of phenol was created by flowing 1.8 bar of helium carrier gas through solid phenol heated to 70°C in the sample tube of a pulsed Even-Lavie valve, operating at a repetition rate of 250 Hz, and expanding the mixture through a 50 μm aperture and 1 mm skimmer into the interaction region of a VMI spectrometer. The molecular beam was intersected with femtosecond laser pulses generated by frequency doubling the output of an optical parametric amplifier (Coherent Opera-F) pumped by an amplified Ti:Sapphire femtosecond laser system (Coherent Verdi, Mira and Legend). The $1/e^2$ pulse durations have been measured to be in the range of 280 - 320 fs at the relevant wavelengths ($\sim$300 fs for 235.5 nm). The flux was attenuated to keep the photoelectron count-rates below 10 photoelectrons per pulse to avoid detector saturation and multiphoton processes occurring and the known binding energy of phenol used to determine no space-charge effects were occurring. Photoelectron images were recorded for 600 s. Background images (without phenol) were also recorded for 600 s and subtracted from the photoelectron images. Photoelectron spectra were recovered from the background-subtracted data using the pBASEX image inversion algorithm and the energy scale was calibrated by recording the $2+1$ resonance-enhanced multiphoton ionisation (REMPI) spectrum of Xe at 249.6 nm. The resolution was $\Delta E/E \approx 3\%$.

1.2 Liquid-jet photoelectron spectrometer

Our liquid-microjet photoelectron spectrometer will be described in detail in a future publication. Briefly, the apparatus comprises a commercial liquid microjet (Microliquids GmbH) and a magnetic-bottle photoelectron spectrometer. A high-performance liquid chromatography (HPLC) pump (Microliquids, 002) was employed to deliver 100 mM aqueous solutions of phenol to a 20 μm diameter fused silica capillary, using a backing pressure of 70 bar and flow-rate of 0.6 ml/min. The phenol solution was prepared using highly demineralised water (conductance, 15 MΩ/cm); 30 mM sodium fluoride was added to minimise charging effects and increase the conductivity of the liquid jet. The liquid-jet was intersected with femtosecond laser pulses 1 mm downstream from the nozzle in the region of laminar flow. The laser pulses were generated by frequency upconverting the output of an optical parametric amplifier (TOPAS) pumped by an amplified Ti:Sapphire femtosecond laser system (Coherent Micra and Legend) operating at 1 kHz. The $1/e^2$ pulse duration of the 235.5 nm pulses was measured to be $\sim$150 fs. The flux was attenuated so that the count-rate was typically 500 Hz (below 1 photoelectron per pulse) to avoid space-charge effects and saturation of the detector. Photoelectrons were collected and analysed using a magnetic bottle photoelectron spectrometer, consisting of a permanent magnet built from two magnetised cylinders of Sm_2Co_{17} and a conical iron cap and a 0.63 m flight tube with a solenoid and a μ-metal shield. The photoelectrons were detected using a microchannel plate (Beam Imaging Solutions) at the end of the flight tube and the photoelectron signal was preamplified and counted using a digitiser (Keysight U5309A). The polarization of the laser was set parallel to the flight axis. The energy scales of the time-of-flight spectra were calibrated by recording one-colour $1+1$ and $2+1$ REMPI spectra of NO. The resolution was $\Delta E/E \approx 2\%$.

1.3 Streaming potential measurement

The liquid-jet is electrically charged due to dynamic separation of the electrical double layers formed around the inner walls of the capillary and the resulting streaming current generates

a streaming potential that accelerates or decelerates photoelectrons emitted from the liquid-jet. The nozzle was passivated for around 26 hours to ensure that the ion-exchange processes responsible for the streaming potential had reached equilibrium before we began measurements and all measurements were made during one afternoon. The streaming potential was measured using a method based on that reported by Tang *et.al.*.[2] Briefly, we recorded the $2+1$ REMPI of Xe at 249.6 nm in the presence of the liquid-jet near the ionisation point of Xe. The resulting shift in electron kinetic energy (eKE) is plotted in Fig. 1 for different distances between the ionisation point of Xe and the liquid-jet, Δx (see inset). The eKE is expressed as

$$eKE(x) = eKE_{\text{field-free}} - \frac{L\phi}{L + \Delta x} \tag{1}$$

where L is the distance between the ionisation point and the skimmer, $eKE_{\text{field-free}}$ is the eKE following 2+1 photoionisation of Xe when the jet is not running and ϕ is the streaming potential. The streaming potential was measured before ($\phi = -0.13$ eV, $R^2 = 0.968$) and after ($\phi = -0.15$ eV, $R^2 = 0.964$) recording the photoelectron spectra. The measurement with the best fit was taken as the streaming potential measurement ($\phi = -0.13$ eV) and was accounted for by adjusting the eKEs derived directly from the time-of-flight measurements.

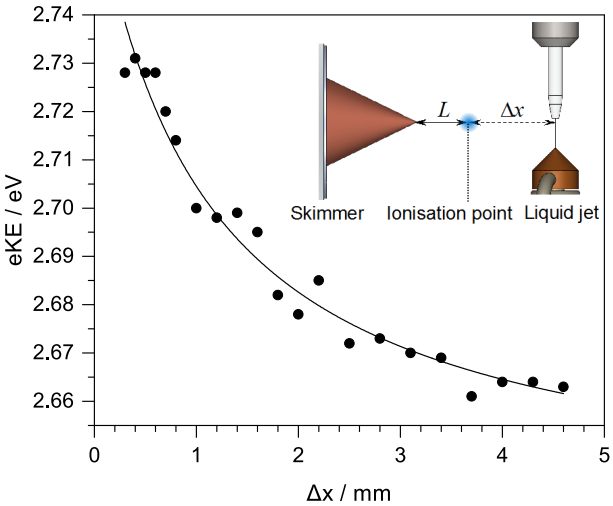

Figure S1: Photoelectron kinetic energy measured as a function of distance Δx between the ionisation point of Xe and the 110 mM aqueous phenol jet (solid circles). Xe was ionised by 2+1 REMPI at 249.67 nm. The solid black line is the least-squares fit of Eq. 1. $L = 1.1$ mm for these measurements.

2 Experimental results

2.1 Photoelectron spectra plotted as a function of two-photon eBE

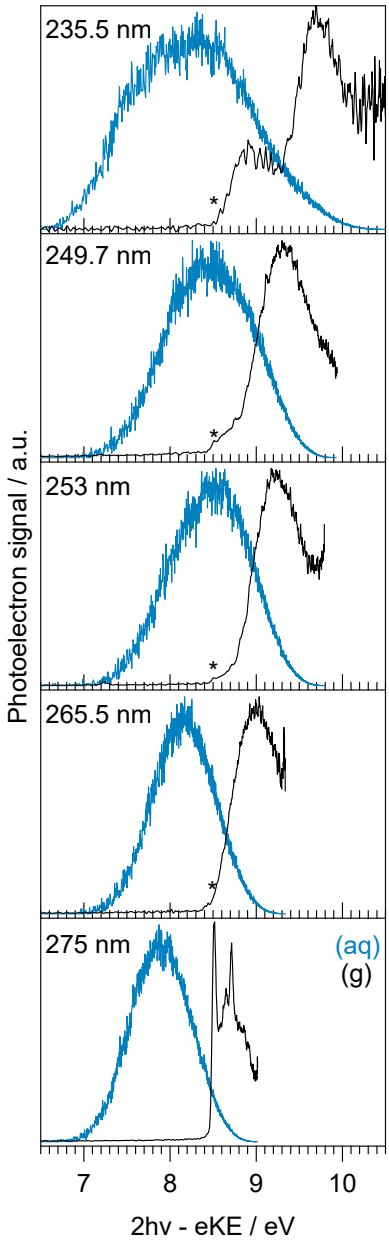

Figure S2: 1+1 UV PES of phenol in the gas-phase (black) and in aqueous solution (blue) recorded following photoexcitation at 275 nm (4.51 eV), 265.5 nm (4.67 eV), 253 nm (4.90 eV), 249.7 nm (4.97 eV) and 235.5 nm (5.27 eV), plotted as a function of two-photon eBE. The asterisks mark the D_0-S_0 AIE and are consistent with the literature value of 8.508 eV.[3]

2.2 Fits to 235.5 nm photoelectron spectra of phenol in aqueous solution

It is possible to fit the spectrum with two Gaussians ($R^2 = 0.9915$) and the fit is only slightly better with three Gaussians ($R^2 = 0.9919$). However, the fit with two Gaussians has peak maxima at 7.4 ± 0.1 eV and 8.3 ± 0.1 eV (two-photon eBEs), which are not consistent with previous BESSY measurements (7.8 ± 0.1 eV and 8.5 ± 0.1 eV),[4] and the higher eBE peak has a one-photon eBE of 3.0 eV, which is far from our measurements of D_0-$1^1\pi\pi^*$ VIE at longer wavelengths (3.5 ± 0.1 eV). On the other hand, the fit with three Gaussians gives peak maxima for processes II and III of 7.6 ± 0.1 eV and 8.5 ± 0.1 eV (two-photon eBEs), that are consistent with the previous BESSY measurements, and the peak at higher eBE corresponds to one-photon eBE of 3.24 eV, which is closer to our measurement of the D_0-$1^1\pi\pi^*$ VIE (process I) at longer wavelengths.

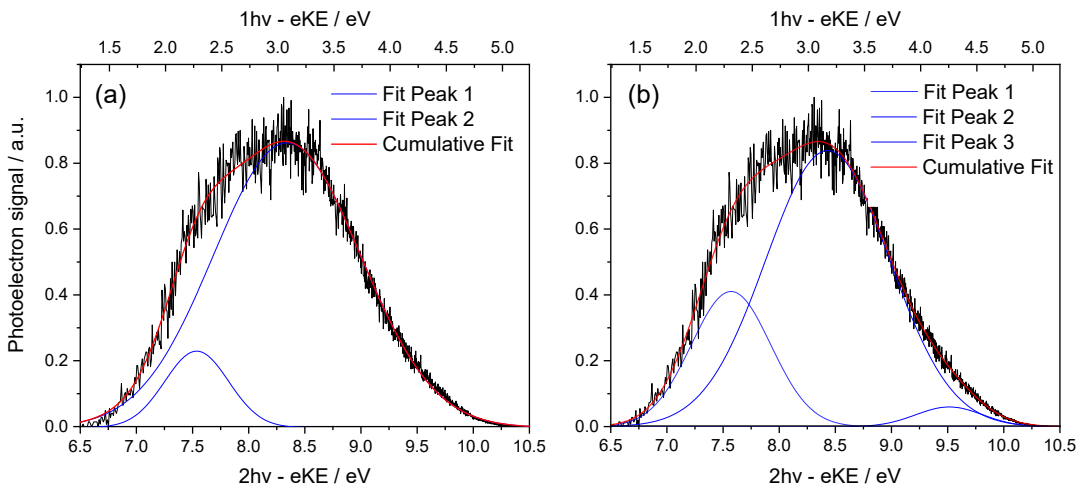

Figure S3: 1+1 UV PES of phenol in aqueous solution recorded following photoexcitation at 235.5 nm and plotted as a function of two-photon eBE (bottom axes) and one-photon eBE (top axes). The experimental spectrum is fit to (a) two Gaussians and (b) three Gaussians.

2.3 Velocity-map images

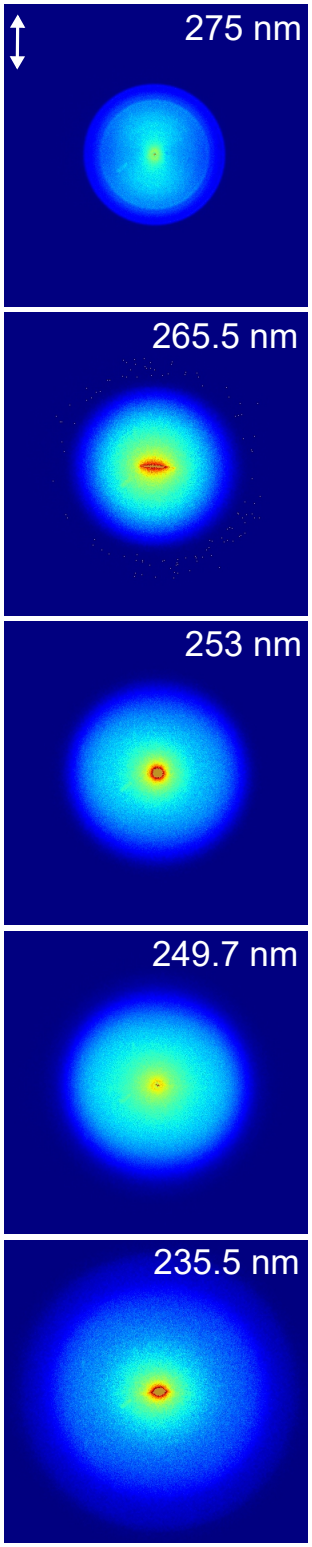

Figure S4: Raw velocity map images recorded for gaseous phenol using the molecular beam velocity map imaging spectrometer. In all images the polarisation axis of the laser is parallel to the double headed arrow (top left).

3 Computational methods

The geometries of isolated phenol and phenol with up to six explicit water molecules were optimised using the Møller-Plesset Perturbation Theory of 2nd Order (MP2) method[5] in the Gaussian09 program suite;[6] for phenol with five or six water molecules, several possible complexes were considered, noted as "clusters" in Figure S5. We did not optimise a cluster with two water molecules, since this would not provide any additional information that was not obtained with the cluster with three water molecules.

Vertical ionisation energies (VIEs) from the ground electronic state were calculated using the equation-of-motion coupled-cluster method with single and double excitations (EOM-CCSD) for the calculation of ionisation potentials (EOM-IP-CCSD).[7] The vertical excitation energy (VEE) for the $1^1\pi\pi^*$-S_0 transition was calculated with the EOM-CCSD method for excitation energies (EOM-EE-CCSD).[7] The VIEs from $1^1\pi\pi^*$ were then obtained as the difference between the VEE and VIE of the relevant D_n-S_0 ionisation. These calculations were carried out using the Q-Chem program package, version 4.3.[8] For all ionisation processes, Dyson orbitals and their corresponding norms[9] were calculated with EOM-IP/EE-CCSD using the Q-Chem CCMAN2 module. In all calculations, the aug-cc-pVDZ basis set was used.[10]

The Dyson orbitals and norms are needed to obtain photoionisation cross-sections with the ezDyson program[11] (version 3.3). Spherical averaged cross-sections were computed for each transition individually. In the ezDyson calculations, a maximum angular momentum number of 5 was applied. The charge of the ionised molecule is +1, hence Coulomb waves were used to describe the electrostatic interaction between the outgoing electron and the charge remaining at the molecule. The cross-sections were computed for a grid of eKEs of the outgoing electrons with a spacing of 0.1 eV. For the reference photoionisation energy, experimental values given in Table S1 were used. Since ionisation takes place from singlet states, a factor of 2 accounting for spin-degeneracy was applied. There are no degenerate orbitals present that would need to be taken into account.

4 Computational results

4.1 Structures of phenol + nH$_2$O

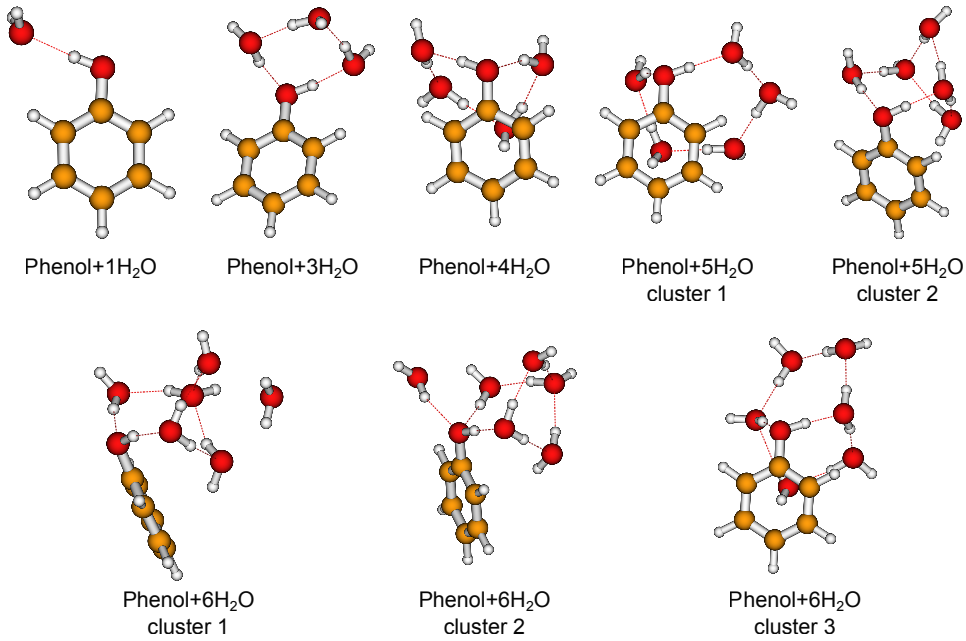

Figure S5: Structures of phenol + nH$_2$O with n = 1, 3, 4, 5 or 6 water molecules. The phenol + 3H$_2$O was first found in reference 12.

4.2 Calculated and experimental IEs and VEEs

	Calculated			Experimental			
Molecule	S_0-D_0	S_0-D_1	S_0-$1\pi\pi^*$	S_0-D_0	S_0-D_1	S_0-$1\pi\pi^*$	$1\pi\pi^*$-D_0
Phenol (g)	8.460[a]	9.285[a]	4.869[a]	8.508[b]	9.36[c]	4.63[d]	4.3 ± 0.1[a]
Phenol (aq)	7.9[e]	8.6[e]		7.6 ± 0.1[a]	8.5 ± 0.1[a]	4.57[d]	3.5 ± 0.1[a]
				7.8 ± 0.1[e]	8.6 ± 0.1[e]		

[a] VIE from this work
[b] AIE from Ref. 3
[c] AIE from Ref. 13
[d] VEE estimated from the maxima of the UV-vis absorption spectra presented in Fig. 1 of this work
[e] VIE from Ref. 4

Table S1: Calculated and measured IEs from S_0 to D_0 (electron hole in π_{HOMO}) and D_1 (electron hole in $\pi_{HOMO\text{-}1}$), calculated and measured VEEs from S_0 to $1\pi\pi^*$ and measured VIEs from $1\pi\pi^*$ to D_0, for phenol in the gas-phase and in aqueous solution. All values are in eV.

4.3 Ionisation cross-sections of phenol + nH$_2$O

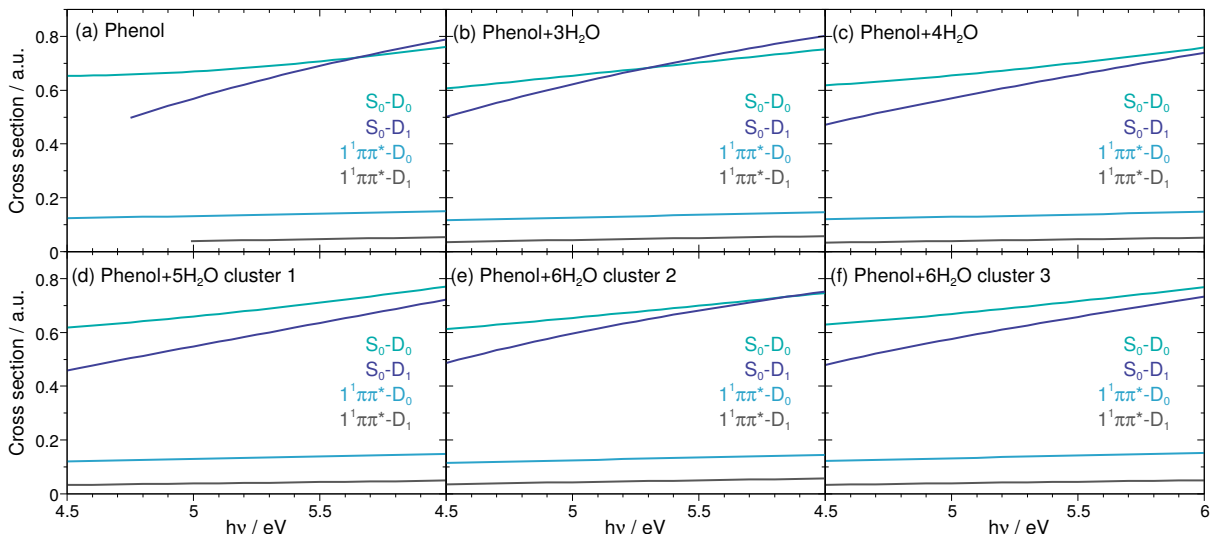

Figure S6: One-photon photoionisation cross-sections for phenol + nH$_2$O. The top two curves in each plot are one-photon photoionisation cross-sections from the S_0 state of phenol to the D_0 and D_1 states of the phenol cation plotted as a function of photon energy for an equivalent two-photon (1+1 non-resonant) ionisation process. The lower two curves in each plot are one-photon photoionisation cross-sections for ionisation from the $1^1\pi\pi^*$ state of phenol to the D_0 and D_1 states of the phenol cation plotted as a function of photon energy.

References

[1] G. A. Worth, R. E. Carley and H. H. Fielding, *Chemical Physics*, 2007, **338**, 220–227.

[2] Y. Tang, Y.-i. Suzuki, H. Shen, K. Sekiguchi, N. Kurahashi, K. Nishizawa, P. Zuo and T. Suzuki, *Chemical Physics Letters*, 2010, **494**, 111–116.

[3] R. J. Lipert and S. D. Colson, *The Journal of Chemical Physics*, 1990, **92**, 3240–3241.

[4] D. Ghosh, A. Roy, R. Seidel, B. Winter, S. Bradforth and A. I. Krylov, *J. Phys. Chem. B*, 2012, **116**, 7269–80.

[5] C. Møller and M. S. Plesset, *Phys. Ref.*, 1934, **46**, 618.

[6] M. J. Frisch, G. W. Trucks, H. B. Schlegel, G. E. Scuseria, M. A. Robb, J. R. Cheeseman, G. Scalmani, V. Barone, B. Mennucci, G. A. Petersson, H. Nakatsuji, M. Caricato, X. Li, H. P. Hratchian, A. F. Izmaylov, J. Bloino, G. Zheng, J. L. Sonnenberg, M. Hada, G. Ehara, M, K. Toyota, R. Fukuda, J. Hasegawa, M. Ishida, T. Nakajima, Y. Honda, O. Kitao, H. Nakai, T. Vreven, J. E. Montgomery, Jr., J. A. Peralta, F. Ogliaro, M. Bearpark, J. J. Heyd, E. Brothers, K. N. Kudin, V. N. Staroverov, R. Kobayashi, J. Normand, K. Raghavachari, A. Rendell, J. C. Burant, S. S. Iyengar, J. Tomasi, M. Cossi, N. Rega, J. M. Millam, M. Klene, J. E. Knox, J. B. Cross, V. Bakken, C. Adamo, J. Jaramillo, R. Gomperts, R. E. Stratmann, O. Yazyev, A. J. Austin, R. Cammi, C. Pomelli, J. W. Ochterski, R. L. Martin, K. Morokuma, V. G. Zakrzewski, G. A. Voth, P. Salvador, J. J. Dannenberg, S. Dapprich, A. D. Daniels, Ö. Farkas, J. B. Foresman, J. V. Ortiz, J. Cioslowski and D. J. Fox, *Gaussian 09, Revision A.1*, 2009.

[7] A. I. Krylov, *Ann. Rev. Phys. Chem.*, 2008, **59**, 433–462.

[8] Y. Shao, Z. Gan, E. Epifanovsky, A. T. Gilbert, M. Wormit, J. Kussmann, A. W. Lange, A. Behn, J. Deng, X. Feng, D. Ghosh, M. Goldey, P. R. Horn, L. D. Jacobson, I. Kaliman, R. Z. Khaliullin, T. Kuś, A. Landau, J. Liu, E. I. Proynov, Y. M. Rhee, R. M. Richard, M. A. Rohrdanz, R. P. Steele, E. J. Sundstrom, H. L. Woodcock, P. M. Zimmerman, D. Zuev, B. Albrecht, E. Alguire, B. Austin, G. J. O. Beran, Y. A. Bernard, E. Berquist, K. Brandhorst, K. B. Bravaya, S. T. Brown, D. Casanova, C.-M. Chang, Y. Chen, S. H. Chien, K. D. Closser, D. L. Crittenden, M. Diedenhofen, R. A. DiStasio, H. Do, A. D. Dutoi, R. G. Edgar, S. Fatehi, L. Fusti-Molnar, A. Ghysels, A. Golubeva-Zadorozhnaya, J. Gomes, M. W. Hanson-Heine, P. H. Harbach, A. W. Hauser, E. G. Hohenstein, Z. C. Holden, T.-C. Jagau, H. Ji, B. Kaduk, K. Khistyaev, J. Kim, J. Kim, R. A. King, P. Klunzinger, D. Kosenkov, T. Kowalczyk, C. M. Krauter, K. U. Lao, A. D. Laurent, K. V. Lawler, S. V. Levchenko, C. Y. Lin, F. Liu, E. Livshits, R. C. Lochan, A. Luenser, P. Manohar, S. F. Manzer, S.-P. Mao, N. Mardirossian, A. V. Marenich, S. A. Maurer, N. J. Mayhall, E. Neuscamman, C. M. Oana, R. Olivares-Amaya, D. P. O'Neill, J. A. Parkhill, T. M. Perrine, R. Peverati, A. Prociuk, D. R. Rehn, E. Rosta, N. J. Russ, S. M. Sharada, S. Sharma, D. W. Small, A. Sodt, T. Stein, D. Stück, Y.-C. Su, A. J. Thom, T. Tsuchimochi, V. Vanovschi, L. Vogt, O. Vydrov, T. Wang, M. A. Watson, J. Wenzel, A. White, C. F. Williams, J. Yang, S. Yeganeh, S. R. Yost, Z.-Q. You, I. Y. Zhang, X. Zhang, Y. Zhao, B. R. Brooks, G. K. Chan, D. M. Chipman, C. J. Cramer, W. A. Goddard, M. S. Gordon, W. J. Hehre, A. Klamt, H. F. Schaefer, M. W. Schmidt, C. D. Sherrill, D. G. Truhlar, A. Warshel, X. Xu, A. Aspuru-Guzik, R. Baer, A. T. Bell, N. A. Besley, J.-D. Chai, A. Dreuw, B. D. Dunietz, T. R. Furlani, S. R. Gwaltney, C.-P. Hsu, Y. Jung, J. Kong, D. S. Lambrecht, W. Liang, C. Ochsenfeld, V. A. Rassolov, L. V. Slipchenko, J. E. Subotnik, T. Van Voorhis, J. M. Herbert, A. I. Krylov, P. M. Gill and M. Head-Gordon, *Mol. Phys.*, 2015, **113**, 184–215.

[9] M. Spanner, S. Patchkovskii, C. Zhou, S. Matsika, M. Kotur and T. C. Weinacht, *Phys. Rev. A*, 2012, **86**, 053406.

[10] R. a. Kendall, T. H. Dunning Jr. and R. J. Harrison, *J. Chem. Phys.*, 1992, **96**, 6796.

[11] C. M. Oana and A. I. Krylov, *Journal of Chemical Physics*, 2007, **127**, 1–14.

[12] T. Bürgi, M. Schütz and S. Leutwyler, *J. Chem. Phys.*, 1995, **103**, 6350–6361.

[13] M. J. S. Dewar and S. D. Worley, *The Journal of Chemical Physics Ionization Potentials of Some Molecules The Journal of Chemical Physics Journal of Chemical Physics Journal of Chemical Physics*, 1969, **50**, year.